Micrite: A Sub-100-Micron Distributed Sensor System

by

Christopher Thomas

A qualifying exam report
submitted to the Faculty of Graduate Studies
in partial fulfillment of the requirements
for the degree of
Doctor of Philosophy

Graduate Program in Computer Science & Engineering
York University
Toronto, Ontario
November 17, 2010

©Christopher Thomas 2010

Contents

1 Introduction **1**

2 System Studies **2**

2.1 Surveillance Systems 3

2.2 Very Small Devices 6

3 Components of Interest **8**

3.1 Integrated Imaging Systems 9

3.2 Low-Power Analog and Digital Circuits 13

3.2.1 Analog to Digital Conversion 13

3.2.2 Image and Data Processing 14

3.3 Wireless Interconnects 16

3.3.1 Short-Range Communication 16

3.3.2 Long-Range Communication 17

3.4 Power Generation, Conversion, and Storage 20

3.4.1 Power Collection and Storage 20
3.4.2 Power Conversion 21
3.5 CMOS-Compatible LEDs 23
3.5.1 Conventional LED Structures 23
3.5.2 Integration With Silicon 25
4 Concluding Remarks **27**

Chapter 1

Introduction

With the widespread availability of compact, inexpensive computing and sensing devices, the field of distributed sensing has seen a great deal of research activity. This work attempts to extend that research to study the fabrication of self-contained sensor devices 100 microns in size and smaller. By analogy with the science fiction term “nanite”, these are dubbed “Micrites”. A popular application for distributed sensing networks is surveillance. Modern research focuses on “third-generation” surveillance systems that perform processing and data reduction within camera or sensor nodes. For purposes of the Micrite project, surveillance is chosen as a target application in order to impose constraints on the design and function of Micrite sensor motes.

Chapter 2 presents an overview of existing work on distributed surveillance networks and on highly-miniaturized sensor platforms. Chapter 3 presents an overview of existing research into the component systems needed for a 100 micron scale sensor mote. Concluding remarks are in Chapter 4.

Chapter 2

System Studies

A major application of distributed sensing systems is surveillance. Published works related to surveillance are described in Section 2.1. As the sensing and data processing tasks associated with surveillance are well-understood and as there is a considerable body of published literature describing these, surveillance will be considered the primary application of Micrite motes for purposes of this project. Other distributed sensing applications have been proposed in the literature; these include weather monitoring, wildlife surveys, and vehicle guidance applications[fact1]. While Micrite sensors may be useful for these applications, they are considered beyond the scope of the present project.

Shrinking distributed sensing systems to sub-millimetre size has many associated challenges. Section 2.2 discusses published works relating to building small, highly-integrated systems with features in common with Micrite motes. These are useful both for highlighting approaches that may be useful in for the Micrite project and for points of comparison in the space of possible implementations.

2.1 Surveillance Systems

The purpose of surveillance systems is to monitor one or more locations in order to detect objects or events of interest. Usually this involves detecting and tracking humans and/or cars and flagging abnormal behavior[1]. Current research on surveillance systems focuses on so-called “third generation” systems, which are highly-distributed systems featuring a large number of sensor nodes with hierarchical processing[2]. Nodes (which may be cameras or other sensors) perform feature extraction on image, sound, or network traffic data and forward event information to a higher-level tier for data fusion and further analysis. This higher tier may also provide individual nodes with more precise estimates of a tracked entity’s properties to assist with subsequent feature extraction attempts. The architecture of a typical third-generation surveillance system is shown in Figure 2.1.

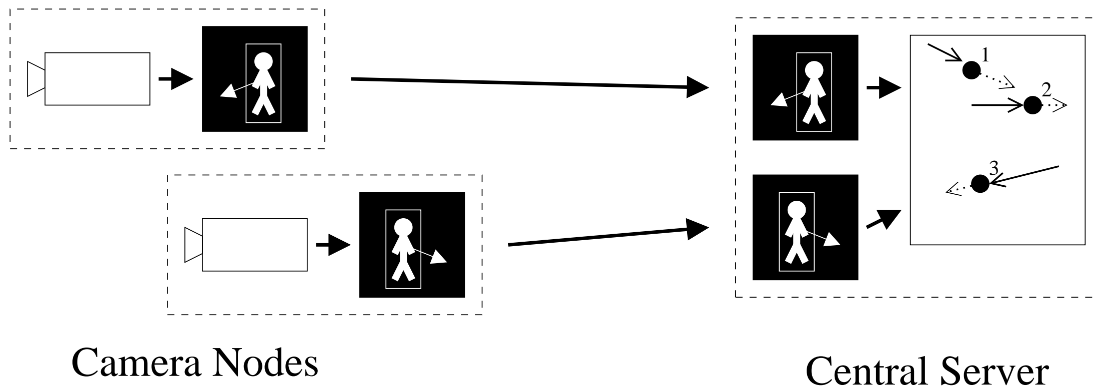

Figure 2.1: Typical third generation surveillance system architecture.

The goal of information processing within third-generation systems is to perform detection, monitoring, and assessment of surveillance targets with minimal human involvement, only presenting to operators data that is considered “interesting”. Three types of data processing are performed, in order to facilitate this: detection of objects of interest, tracking of objects of interest, and evaluation of object behaviour (so that behaviour flagged as “abnormal” can be brought to supervisor attention). There are many approaches to performing this processing[3]; a typical processing flow is shown in Figure 2.2[4].

One of the defining characteristics of a third-generation surveillance system is offloading of some or all of the recognition and tracking task components to individual camera nodes[5]. This serves the

Figure 2.2: Typical data processing flow in a third-generation surveillance system.

dual purposes of reducing processing load on the central server and reducing network traffic (by performing data reduction in the "smart camera" nodes)[4]. Typical "smart camera" implementations are VGA or higher-resolution cameras equipped with local DSP or FPGA hardware[6], though implementations using conventional cameras connected to dedicated computers also exist[7][8]. Typical processing steps implemented by a "smart camera" include distinguishing foreground pixels from background pixels (via colour[9][7][8], combined colour and depth data[10][11], or time differencing[12]), grouping of foreground pixels into "blobs" that represent individual objects to be tracked[10] with bounding box and centroid information extracted, extraction of colour histogram information for object classification[13][10][7][8], filtering of image pixels for both low-level processing (edge detection, noise reduction) and for object recognition (identification and tracking via Hough transform variants[14], face extraction via Haar-like features[15]), and trajectory estimation for tracked objects (for robustness against occlusion or intermittent detection).

Operations that are centralized in smart camera systems include automated estimation of degree of overlap or occupancy correlation between camera fields of view[16][17] and globally-directed pruning of targets being tracked within individual camera nodes[18]. The purpose of automated estimation of camera field of view correlation is to reduce the amount of manual calibration needed for cameras, which becomes important when a very large number of cameras is in place[16]. The purpose of removing targets from tracking lists within cameras is to conserve smart camera resources, allocating resources only from cameras that have the best views of any given target.

For purposes of this research project, Micrite motes are considered to be smart camera nodes with low-resolution cameras, minimal processing resources (due to power constraints), and minimal communication resources (also due to power constraints). Image processing algorithms of interest for the Micrite project are those which can perform a large amount of data reduction with a modest amount of processing power, possibly at the expense of accuracy of tracking or detection. Implementation of processing and control functions higher in the camera hierarchy are left for future research.

2.2 Very Small Devices

The idea of extremely small sensors (and even extremely small robotic devices) has been a staple of science fiction for decades. More recently, self-contained sensors and robotic devices on a centimetre or millimetre scale have been proposed in academic literature, and in some cases actually built and tested.

The "Smart Dust" project undertaken by the University of California at Berkeley most closely resembles the design of Micrite motes. The goal of the Smart Dust project is to produce motes that fit within one cubic millimetre[19]. Unlike Micrite motes, these are only partly-integrated. They are intended to be assembled from several discrete components, the largest of which is a thick-film battery for power storage. Use of multiple fabrication processes also allows easier integration of high-efficiency photovoltaic cells, diode lasers, and movable MEMS optical elements into the system. Power generation is photovoltaic, power storage is via a battery and a discrete capacitor, and communication is optical, with both a modulated corner-cube reflector (CCR) passive scheme and active diode laser and LED transmission schemes available[20]. A prototype without a battery and with only a CCR transceiver was constructed with a volume of 16 cubic millimetres[21].

The "COTS Dust" project is a spinoff of the Smart Dust project that involves prototype devices several centimetres in size[22]. The goal of the COTS Dust project is to provide a platform on which software and sensing tasks can be tested in parallel to development of millimetre-scale Smart Dust hardware. Several of the issues that are relevant to Micrite motes were noted in the COTS Dust publications (in particular, the importance of power management and the difficulty of using radio-frequency communication with devices of millimetre scale or smaller).

Another project with similarities to proposed Micrite motes is an integrated system produced at the Moscow University of Electronics and Mathematics[23]. This device was a fully-integrated smart sensor/controller mock-up interrogated and powered by a laser or other bright light source. While return signalling was via an external component (a liquid-crystal element), all other components and functions for a self-contained system were integrated on to one die.

In addition to hardware concerns, software[24] and communication protocol[25][26] concerns have

been studied as issues affecting large networks of very small devices. While relevant to the Micrite project, these design aspects are considered beyond the scope of the present research project.

Chapter 3

Components of Interest

Sensor devices on the 100 micron scale have to operate with an energy budget on the order of 1 pJ or less, and have to consist of components that can either be fabricated using conventional commercial semiconductor lithography processes or that can be easily integrated into such processes. Several research projects exist that either describe such components or point in useful directions. Section 3.1 discusses integrated imaging systems of interest, Section 3.2 discusses analog to digital conversion and data processing, Section 3.3 discusses several wireless interconnect schemes that are applicable to mote communication, Section 3.4 discusses power generation, conversion, and storage, and Section 3.5 discusses CMOS-compatible light-emitting diode structures for communications use.

3.1 Integrated Imaging Systems

Micrite motes must be able to sense their environment. For surveillance applications, the most important sensing mode is greyscale imaging, followed by the ability to detect colour information in images. In a conventional imaging system, shown in Figure 3.1a), external optics form an image on an integrated circuit sensor, optionally with colour filters and additional concentrating optics on-die[27][28][29]. A fully-integrated on-die imaging system, shown in Figure 3.1b), does not have external optics available. On-die optics are used for image-forming, and specialized layers such as colour filters might not be available. Fabrication of on-die optical elements is the main challenge for implementation of Micrite image sensing, as other image sensor components are well-understood and readily implemented with unmodified CMOS processes.

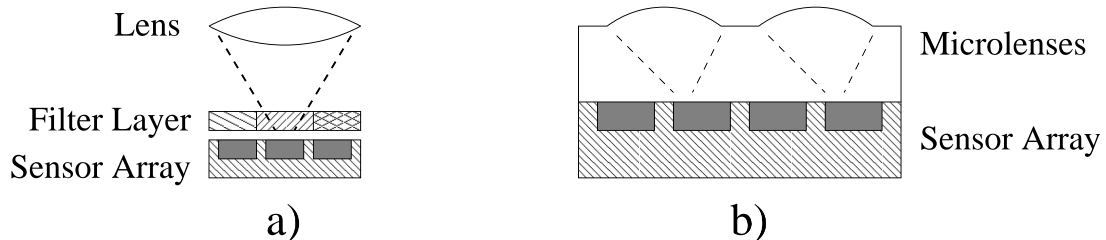

Figure 3.1: Conventional and fully-integrated imaging systems.

The most common integrated optical element is the microlens. Many approaches to microlens fabrication have been studied; typical examples are shown in Figure 3.2. Figure 3.2a) shows microlenses transferred from a conformal mold[30], Figure 3.2b) shows microlenses formed by resist reflow[31], and Figure 3.2c) shows microlenses formed by sacrificial etching of a template patterned in resist[32]. In addition to being widely used as concentrating elements, microlenses have been used in standalone integrated systems for imaging[33][34] and as imaging components in a Hartmann-Shack wavefront sensor (which measures deflection of spots imaged from plane waves)[35]. Microlenses have also been used as beam-forming elements for single-die LED arrays[36].

As an alternative to refractive microlenses, several types of diffractive optical element have been studied. These are depicted in Figure 3.3. Transmissive optics, shown in Figure 3.3a), work by patterning a material with a high refractive index in order to phase-shift incident light. Examples

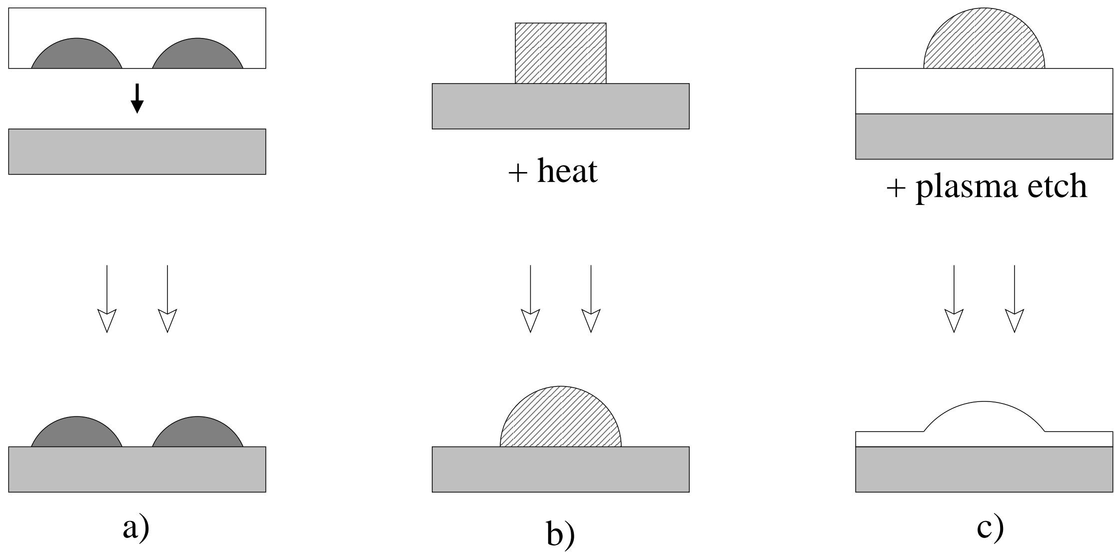

Figure 3.2: Microlens fabrication methods.

include Fresnel zone plates etched into GaN[37][38], anti-reflective textures etched into diamond[32], and holographic gratings etched into silica[39]. An adaptive variant using a liquid crystal pixel array to mask portions of the beam with unwanted phases has also been proposed[40]. Reflective optics, shown in Figure 3.3b), work by adjusting the distance of reflective elements to perform phase shifting of reflected light. Several examples using MEMS reflective elements have been proposed for spectral filtering[41][42], Fresnel zone plate mirrors[43], and general-purpose holographic reflective gratings[40]. Preliminary work for the Micrite project included similar elements using fixed metal structures for transmissive Fresnel zone plate gratings and masks[44][45]. These structures are shown in Figure3.3c). As diffractive optical elements have point spread functions that are sensitive to wavelength and as metal optical elements have point spread functions that are sensitive to polarization, some colour and polarization information from the image may be recoverable by deconvolution using metal-grating optics[45][46].

As mentioned at the beginning of this section, photosensor elements (implemented beneath an imaging system's optics) are also well-studied. Several variants of these are depicted in Figure 3.4. The most widely used type of sensor, the CMOS active pixel sensor (APS), is shown in Figure 3.4a), may be implemented in unmodified silicon CMOS processes. This device consists of a floating photodiode that is charged to reverse bias, and discharged by light-generated carriers. The most

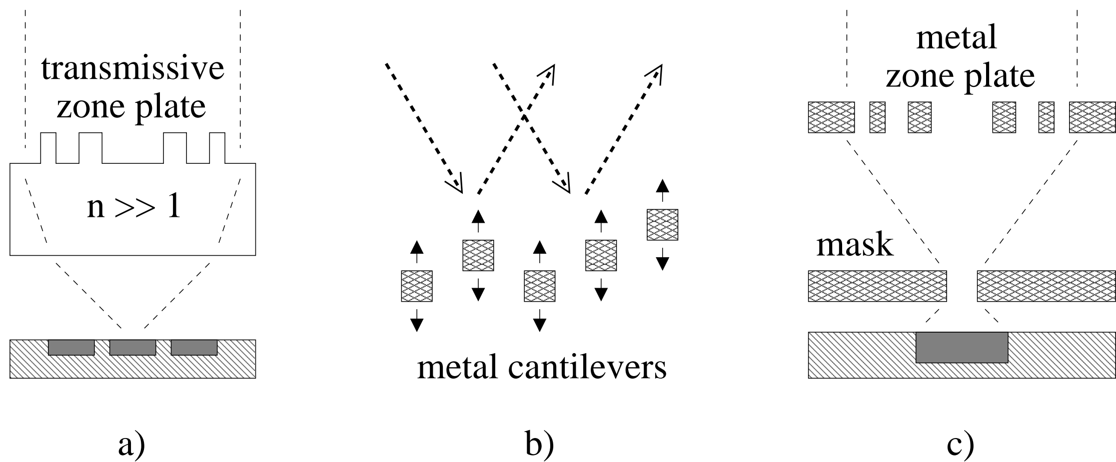

Figure 3.3: Diffractive optical elements.

popular implementation of the CMOS APS (the three-transistor architecture**fact2**) uses a source follower to relay the buffered photovoltage to column bus lines. A second type of sensor that is still widely used is the charged coupled device (CCD), shown in Figure 3.4b). This device uses FET gates to create an inversion region in which photogenerated charge is stored. Voltages on a chain of such gates are manipulated to move the inversion region and shift the stored charge to the end of a sensor row or column for analog-to-digital conversion**fact3**. Lastly, a third type of sensor called an avalanche photodiode is used when extremely high sensitivity is required. This device, shown in Figure 3.4c), is reverse-biased past the avalanche breakdown point. Photogenerated carriers entering the depletion region trigger breakdown, and the resulting current pulse is detected by pixel electronics[47][48].

While colour sensitivity is usually performed by applying a patterned filter over the image sensor array, photosensors can also be designed that determine the colour of incident light directly. This is usually achieved by taking advantage of the fact that different wavelengths of light propagate different distances through silicon, generating different carrier density profiles with respect to depth**fact4**. Figure 3.4d) shows a pixel that stacks several reverse-biased diode junctions, measuring photocurrents from many depths**fact5**. An alternate approach is shown in Figure 3.4e). In this system, the currents in photodiodes with different biases or photodiodes with and without shielding are compared to discriminate between carriers originating near the surface and deeper carriers that

diffuse laterally through the substrate[49][50].

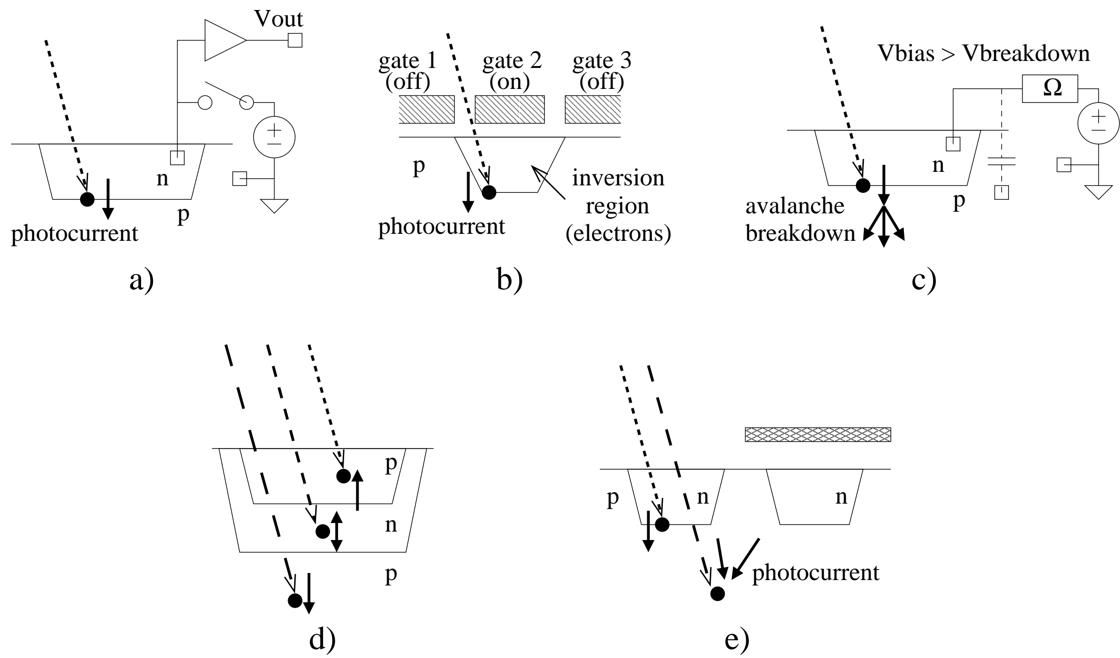

Figure 3.4: Photosensor implementations.

3.2 Low-Power Analog and Digital Circuits

3.2.1 Analog to Digital Conversion

The most important and most energy-intensive analog operation performed by a Micrite mote is analog to digital conversion. Analog to digital conversion is performed both on image sensor signals and on communications receiver signals. In the case of image signals, high precision digitization is very useful, as many image processing operations (such as convolution) function poorly in the presence of noise. In the case of communications, lower precision is acceptable, as only the presence or absence of a communication signal (against a background) is of interest. Conversion of image processing signals is therefore likely to be the most expensive analog operation performed.

Typical analog to digital converter (ADC) architectures are shown in Figure 3.5. All of these have merits and drawbacks. Flash converters provide output in one comparator settling time, but require 2^n comparisons for n bits of precision, and a large amount of space (for 2^n comparators). Sub-ranging converters require $O(n)$ comparisons for n bits of precision, but also require n very precise amplification steps during conversion. Successive approximation converters take n steps per conversion, but require n DAC (digital to analog conversion) operations during this process. These DAC stages typically require either a large amount of current (up to 2^n times the minimum branch current for a current-steering DAC) or a large amount of area (2^n times the unit capacitor area for a charge redistribution DAC). Sigma-delta converters require $2^{\alpha n}$ steps for n bits of precision, thus taking both a large amount of time and a large amount of energy.

Low power ADCs in published literature are usually optimized for both power and precision, as opposed to having low power as the overwhelming design constraint. These publications can still provide a useful upper bound on the amount of energy needed per sample conversion with a given ADC architecture. A sub-ranging ADC built with 65 nm process technology achieved 45 pJ per sample with 10 bits of precision[51]. A successive approximation ADC using a charge redistribution DAC proposed for Smart Dust prototypes performs an 8-bit conversion using 31 pJ per sample[52]. A different successive approximation ADC with charge redistribution built with a 65 nm process achieved 19 pJ per sample with 10 bits of precision[53]. By comparison, a sub-ranging ADC built

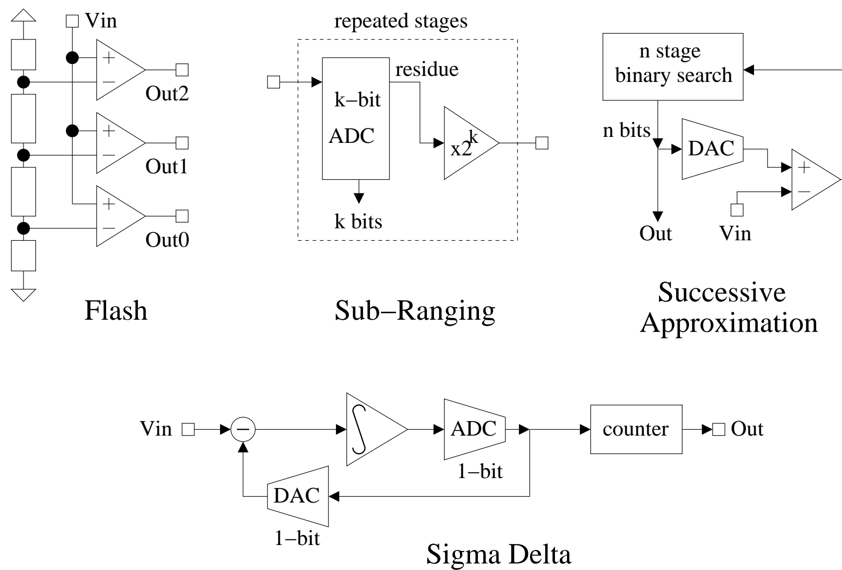

Figure 3.5: Analog to digital converter architectures.

using 0.18 micron process technology similar to that available for the Micrite project used 198 pJ per sample for a 10-bit conversion[54]. These values are typical of those reported in Murmann's survey[55], with the best reported values as of 2010 being about 1 pJ per sample at 4-9 bits per conversion.

3.2.2 Image and Data Processing

For purposes of the Micrite project, image processing and other data processing operations are assumed to occur in the digital domain. The amount of energy required for processing operations is very dependent on the nature of the processing that is being performed. For estimation purposes, the published model data from the semiconductor foundry being used for the Micrite project can be used to calculate approximate estimated power consumption prior to detailed design and simulation of computational elements. According to TSMC's 0.18 micron process information, the dominant parasitic capacitance within circuit nodes is FET gate capacitance, at approximately 1 fF per square micron[56][57]. For purposes of rapid estimation, a node is assumed to be connected to one square micron of transistor gates and to use a rail voltage of 1 V, for an average of 0.25 fJ consumed per node with a 50% activity rate. An addition operation may require dozens of node operations

and a multiplication operation may require hundreds or thousands.

For comparison, a mixed-signal multiply-accumulate engine constructed with 0.5 micron CMOS claims 0.9 pJ per operation (multiplying 4-bit arguments and accumulating the result with 8-bit precision)[58]. Advanced versions of the same engine built with 0.35 micron CMOS and using adiabatic charge recycling claim 5.7 fJ and 2.0 fJ per multiply-accumulate operation[59][60].

A detailed literature survey of ultra-low-power image processing engines is beyond the scope of this project. For purposes of estimation, it can be assumed based on the publications cited that multiplications may require up to 1 pJ of stored energy to perform on Micrite motes.

3.3 Wireless Interconnects

Micrite motes must be able to communicate with a base station, possibly via other Micrite motes. While the base station can have arbitrary communications equipment, communications components on a Micrite mote must be suitable for integration on to a 100 micron die. Communication between devices on similar scales has been widely investigated. Section 3.3.1 describes applicable short-range communication schemes, and Section 3.3.2 describes long-range communication schemes.

3.3.1 Short-Range Communication

Short-range communication (communication on the scale of the device size or smaller) has been studied for use with on-die interconnects and interconnects between chips in a multi-chip module. Typical schemes are depicted in Figure 3.6.

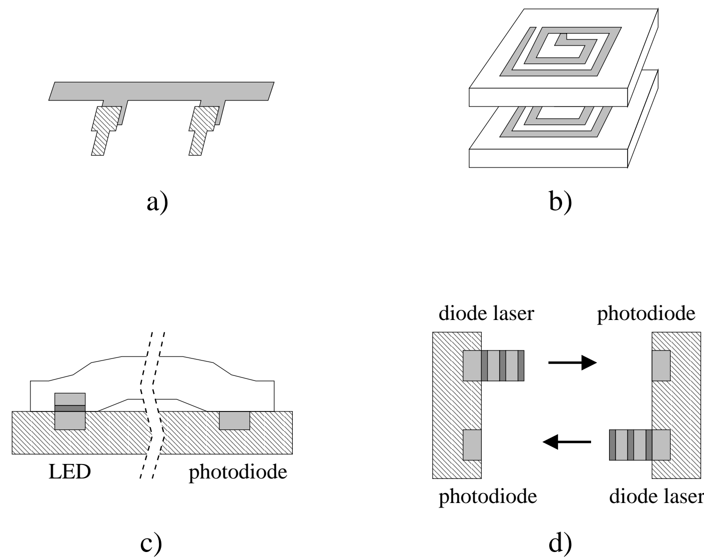

Figure 3.6: Typical short-range communication schemes.

Figure 3.6a) shows a capacitively coupled scheme where devices communicate using a shared multi-drop bus. This is typically proposed for printed circuit board interconnects[61][62][63] or multi-chip module interconnects[64][65][66][67]. Point-to-point variants (connecting only two devices) have also been proposed[68]. Due to capacitive coupling, only AC signal components are transmitted;

transmission of long stretches of low or high levels requires either use of an encoding scheme with frequent transitions or a zero-wander cancellation scheme [69].

Figure 3.6b) shows an inductively coupled scheme where stacked chips communicate using overlapping inductors. This has been proposed for three-dimensional integration[70], though careful design and choice of modulation scheme are required to reduce crosstalk in arrays of inductors[71][72].

Optically coupled interconnect schemes are shown in Figures 3.6c) and 3.6d). Waveguide-coupled schemes using light-emitting diodes for transmission and photodiodes for reception have been proposed for on-die signalling[73] and signalling within multi-chip modules[74]. Free-space interconnect schemes using vertical-cavity diode lasers for transmission and photodiodes for reception have been proposed, in conjunction with external optics, for construction of optoelectronic processing devices[75].

3.3.2 Long-Range Communication

Long-range communication schemes (communication over distances much larger than the sensor device size) have been proposed for sensors of various scales. Typical schemes are depicted in Figure 3.7.

Figure 3.7a) shows a broadcast RF scheme operating in the far field (distances of many wavelengths and larger than the transceiving antennae). These systems have been proposed for communication among surveillance cameras (via wireless networking)[**fact6**] and for communication with remote sensing devices in other contexts[**fact7**] While the base station's antenna can be on the scale of the broadcast wavelength (in the case of a half-wave dipole) or larger (in the case of a dish), a 100 micron Micrite mote is much smaller than any reasonable radio or microwave wavelength (100 GHz microwaves have a wavelength of about 3 mm). As coupling efficiency to an antenna or coil is proportional to the square of the aperture area in this regime[**fact8**], a broadcast RF system might be usable for transmission from a base station to Micrite motes but is not feasible as a means of two-way communication for purposes of the Micrite project.

Figure 3.7b) shows a near-field RF communication scheme. These systems operate over a distance

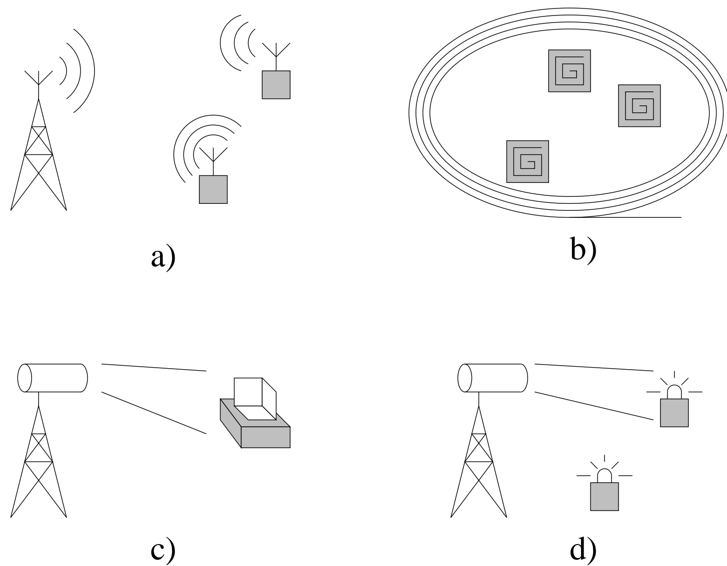

Figure 3.7: Typical long-range communication schemes.

less than one RF wavelength, with a large base station antenna or coil. Systems with this type of configuration have been widely studied in the form of RFID tags and readers[fact9] Transmissions from the base station are received by an antenna on the sensor device. Return communication is implemented by load modulation, with the sensor device altering the impedance - and therefore power draw - of its antenna. As the device is operating in the near field of the transmitting antenna, the transmitting and receiving antennae are coupled strongly enough that a changing receiver load can be detected as a changing power draw in the antenna. Typical systems are centimetres in size, but systems on the scale of Micrite motes have been demonstrated[fact10].

Figure 3.7c) shows a passive optical communication scheme. Systems of this type use a laser and optics in the base station to transmit modulated light to the sensor device. The sensor device does not have the ability to emit light itself, but instead uses a corner cube reflector to return light to the base station. A typical two-way communication scheme uses a MEMS micromirror for one face of the reflector. Movement of this mirror switches between retroreflective and non-retroreflective states, producing a change that can be detected by the base station[fact11].

Figure 3.7d) shows an active optical communication scheme. Systems of this type use a laser and optics in the base station to transmit to the sensor device, and use diode lasers or LEDs in the sensor

device to emit light that the base station's telescope can detect[fact12]. Alternatively, motes with strong enough light generation or close enough proximity can communicate as an ad-hoc network amongst themselves[fact13].

3.4 Power Generation, Conversion, and Storage

The power subsystem of a Micrite mote has three tasks: acquisition of energy from some external source, storage of energy, and conversion of stored energy to voltages that are useful to the other analog and digital subsystems on the mote.

3.4.1 Power Collection and Storage

Two methods of power collection have been widely used: collection from light via photovoltaic cells, and collection from radio-frequency excitation via an inductive pickup coil. RF power is widely used for radio-frequency identification (RFID) tags[fact14] Inductors are external components, with sizes ranging from centimetres to millimetres. This gives them a large enough aperture size for the induced voltage across the inductor's terminals to be large enough to rectify. A few noteworthy exceptions to this size scale exist, including a configuration of Hitachi's mu-chip RFID with a coil size of 400 microns[fact15], but this device must be within millimetres of a reader pickup in order to function in this configuration. RF is not considered a viable means for supplying power to Micrite motes, as Micrite motes are vastly smaller than feasible RF carrier wavelengths (100 GHz microwaves have a wavelength of about 3 millimetres).

Power collection via photovoltaic cells, by contrast, is readily implemented on a Micrite mote scale. Blue photons have penetration depths of less than one micron in silicon, while other photons in the visible range have penetration depths on the order of 10 microns or less (with the exception of the far end of the red portion of the spectrum)[fact16]. Charge generated from photocurrents accumulates in the photodiode's parasitic capacitance, reaching equilibrium when the diode is forward-biased to the point where the forward conduction current equals the photocurrent. This means of power generation has been used by multiple existing projects[23][21], in some cases with an external capacitor for power storage[21].

Power storage is a concern for the Micrite project, as on-die parasitic diode capacitance is about 0.1 fF per square micron and on-die parasitic FET gate capacitance is about 1 fF per square micron[56][57]. Structures available via other processes include DRAM trench capacitors[fact17],

thick-film capacitor process layers[fact18], and thick-film battery layers[fact19]. These are out of scope for the present project, but may become attractive if power storage is a crippling problem for Micrite-scale motes.

3.4.2 Power Conversion

Power received from photovoltaic cells is at a relatively low voltage (approximately 0.5 V per cell for silicon photocells, determined by the forward-biased voltage of the cells at the supplied current)[fact20]. Power received via RF may also be at low voltage, due to the poor coupling efficiency of antennae or pickup coils much smaller than a wavelength in size. This received voltage must be boosted to levels suitable for running analog and digital circuitry on the mote. While digital circuitry in the target process may function with a supply voltage as low as 500 mV[56][57], analog circuitry with rail-to-rail operation requires at least two gate thresholds to function[fact21]. For purposes of the Micrite project, this is assumed to be about 1 V. LEDs, if implemented (per Section 3.5), would have a forward voltage of 2.4 to 3.3 V depending on materials. For purposes of the Micrite project, LEDs are assumed to require a supply of at least 3 V.

If fabrication processes allow construction of floating diodes, as is the case with silicon-on-insulator (SOI) technologies, then transforming photovoltaic voltages is straightforward: several cells can be wired in series. Depending on the photodiode implementation, additional biasing can be performed using boosted voltages to increase the the efficiency of photovoltaic conversion[23]. Bulk CMOS processes are more difficult to perform boosting in, due to parasitic bipolar transistor structures. When illuminated, these act as phototransistors, shorting the diode to the substrate's potential. Under these conditions a charge pump is required.

RF power received via an inductive pickup may similarly require boosting. While pickup coils could be connected in series, this produces no benefit, as the electromotive force across a coil's terminals is proportional to its inductance (and hence, area) for a constant number of windings (already assumed to be maximized). Since the drive frequency is well known, however, some boosting is possible through use of a resonant transformer structure[76].

In the absence of series photodiodes, and possibly even in their presence, chip supply voltages may need to be boosted. The usual way to do this is to use a charge pump. Examples of charge pumps are shown in Figure 3.8. The classic charge pump design proposed by Dickson is shown in Figure 3.8a)[77]. For CMOS implementations, diodes are replaced by diode-connected FETs. This design has difficulty when the input voltage approaches the diode forward voltage, due to the diode drop between stages of the charge pump. Modern charge pumps and voltage doublers avoid the problem by using FET switches driven by boosted voltages, rather than diodes, to regulate current flow. An example of this style of charge pump is shown in Figure 3.8b)[78].

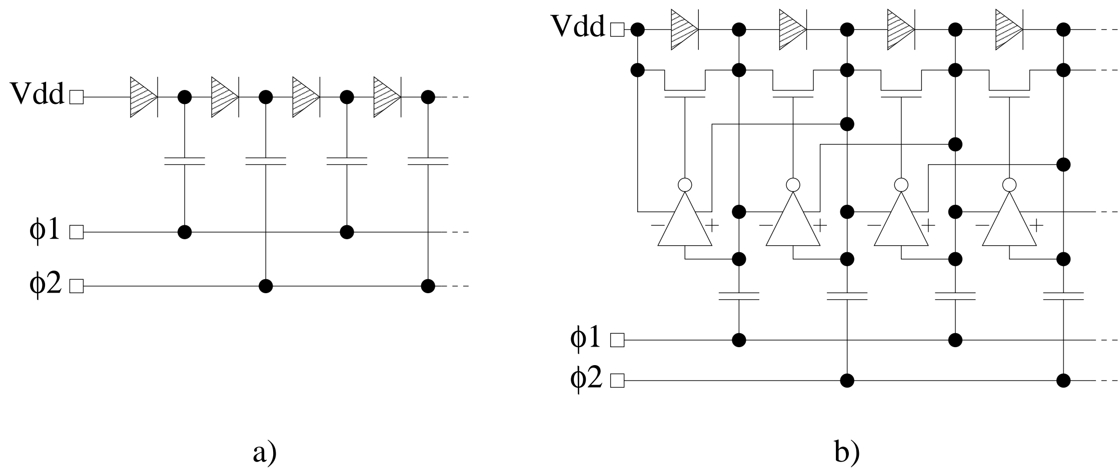

Figure 3.8: Charge pump architectures.

3.5 CMOS-Compatible LEDs

CMOS-compatible LEDs are of interest for communication between motes and communication from motes to base stations. Optical transmitter and receiver elements can be easily miniaturized, and can perform communication between distant transceivers. Capacitive and inductive communication approaches, by contrast, work best in the near field (per Section 3.3. Far field coupling efficiency is very poor.

Optical receiver elements compatible with silicon CMOS technology are widely used. One of the most common implementations is the silicon photodiode receiver used in silicon-based CMOS active pixel sensors, with a pixel pitch as small as 2-4μm[79][80][27][81]. While miniature LEDs with a device pitch of 30 microns[82] and 22 microns[83] have been implemented, LED transmitting elements are difficult to fabricate on silicon substrates. Silicon itself is a poor emitter of light, due to its indirect bandgap, and direct-bandgap materials are difficult to integrate with silicon processes.

3.5.1 Conventional LED Structures

Conventional LEDs are manufactured using AlGaInP on GaAs wafers (for red through green LEDs)[84], or GaN on sapphire or SiC wafers (for blue and UV LEDs)[85]. Both of these compounds are direct-bandgap semiconductors, which means that charge recombination usually results in light emission (with an internal quantum efficiency of about 70% to 80%[**fact22**]).

As shown in Figure 3.9, modern LEDs use a PIN diode architecture using semiconducting alloys with varying bandgaps. Carriers recombine in the intrinsic region, emitting light. In order to prevent light absorption by the N and P doped regions of the diode, these are made from higher-bandgap materials, which are transparent to light emitted at the bandgap energy of the intrinsic region's semiconductor. The top electrode of the photodiode is typically a transparent conductor, most commonly indium tin oxide (ITO), and the bottom electrode is typically metal.

Modern LEDs have several additional features intended to improve the efficiency of light generation

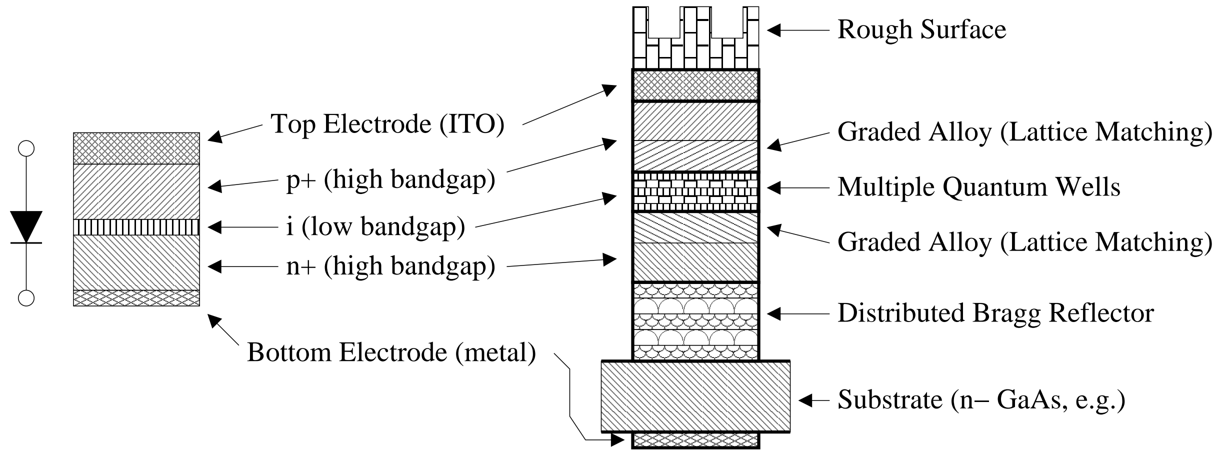

Figure 3.9: Typical high-efficiency LED structure (many variants exist).

and to improve the coupling of light to the outside environment. These are characterized by internal quantum efficiency (the fraction of carrier pairs that are converted to photons) and external quantum efficiency (the fraction of carrier pairs that are converted to photons that exit the LED). In order to improve the efficiency of photon generation, the intrinsic region is a multiple quantum well (MQW) structure formed of thin layers of low-bandgap and high-bandgap semiconductor. Confinement of carriers within low-bandgap quantum wells enhances light emission[**fact23**]. In order to reduce mechanical stress and defects due to lattice mismatch, the composition of the semiconductor is varied (graded) with distance from the junction, so that a sharp transition in composition (and lattice spacing) doesn't occur. In order to reduce losses due to light striking the opaque back electrode, a distributed Bragg reflector (DBR) structure is added between the intrinsic region and the back electrode, formed from repeating layers of semiconductors with different refractive indices with thicknesses chosen so that reflected light constructively interferes with itself[86][87]. In order to narrow the frequency range of emitted light, a second distributed Bragg reflector is sometimes added above the LED to form a resonant cavity[88]. In order to reduce internal reflection at the top of the transparent electrode, rough features are added at the surface of the LED so as to present surfaces through which photons emitted in non-vertical directions can escape[89][90].

3.5.2 Integration With Silicon

Integration of LEDs with Micrite mote circuits requires either fabrication of LEDs on silicon wafers, or fabrication of sensor, logic, and RF circuits on LED wafers. Fabrication of GaAs logic circuits in conjunction with AlGaInP LEDs has been demonstrated on GaAs wafers[91]. Fabrication of InAs transistors suitable for logic on InP wafers (which are also used as an LED and photodiode substrate) has also been demonstrated[92]. However, fabrication on silicon is preferable due to the large amount of industry infrastructure focused on that substrate.

Fabrication of GaN LEDs and high-electron-mobility transistors (HEMTs) on Si wafers has been demonstrated [93][94][95]. These may use the (111) silicon orientation, with poor lattice matching to GaN, or the (100) orientation, with better matching. In both cases, a set of buffer layers several hundred nanometres thick is grown to reduce defects due to lattice mismatch. As well-matched (100) wafers are readily available for integrated circuit fabrication, this is an attractive future option for Micrite mote transmitters. Fabrication of AlGaInP LEDs on silicon has also been attempted. Some efforts involve wafer-bonding[96], which is poorly suited to making sub-100μm devices. Other efforts involve growing a GaAs substrate on top of a Si wafer, through use of a SiGe graded-alloy buffer layer varying from 100% Si at the substrate to 100% Ge at the interface with the GaAs layer[97].

A subject of interest within the last 10-20 years has been light emission from silicon. This is difficult, as due to silicon's indirect bandgap, recombining carriers usually generate lattice vibrations rather than light. Some silicon structures do emit light under the right conditions; emission from avalanche diodes has been documented[98], and on-die optical interconnects have been prototyped using this effect[73].

Most of the recent research on light emission from silicon has been focused on silicon nanocrystals. These widen the bandgap and encourage radiative recombination due to quantum confinement effects when carriers are confined to a region smaller than are smaller than 4-5 nm[99]. Early efforts used nanocrystals embedded within silicon dioxide ("silicon-rich silicon oxide") [100][101]. Use of the oxide had a side effect of pinning emission wavelengths to infrared regardless of nanocrystal

size, due to pinning of one or both carriers to a silicon-oxygen double-bond[102]. More recent efforts have achieved higher efficiency and size-dependent wavelength emission using silicon nanocrystals embedded in silicon nitride[103][104]. This type of LED could be readily integrated with CMOS logic; its drawback is lower emission efficiency than GaN or AlGaInP LEDs[fact24]

Chapter 4

Concluding Remarks

In conclusion, a sufficient body of work exists to make the construction of 100 micron sensor devices potentially feasible. This is a largely-unexplored section of design space, which has recently become accessible due to advances in commercial integrated circuit fabrication methods. The sensing and image processing tasks associated with surveillance are an area of active research that matches well with the potential capabilities of a Micrite style sensor mote, and so this set of tasks is chosen as the designated application of a proof of concept Micrite design.

The goal of this research will be to determine how much of the necessary functionality is feasible to implement with off-the-shelf integrated circuit fabrication technology, and to identify areas where further research into custom fabrication steps or altered design constraints would make Micrite devices more functional.

Bibliography

[1] M. Valera and S. A. Velastin, "Intelligent distributed surveillance systems: a review," *IEE Proceedings - Vision, Image and Signal Processing*, vol. 152, no. 2, pp. 192–204, 2005.

[2] T. D. Raty, "Survey on contemporary remote surveillance systems for public safety," *IEEE Transactions on Systems, Man, and Cybernetics, Part C*, vol. 40, no. 5, pp. 493–515, 2010.

[3] H. Buxton, "Generative models for learning and understanding dynamic scene activity," in *First International Workshop on Generative Model-Based Vision*, 2002, pp. 71–81.

[4] L. Marcenaro, F. Oberti, G. L. Foresti, and C. S. Regazzoni, "Distributed architectures and logical-task decomposition in multimedia surveillance systems," *Proceedings of the IEEE*, vol. 89, no. 10, pp. 1419–1440, 2001.

[5] E. Norouznezhad, A. Bigdeli, A. Postula, and B. C. Lovell, "A high resolution smart camera with gige vision extension for surveillance applications," in *Second ACM/IEEE International Conference on Distributed Smart Cameras*, 2008, pp. 1–8.

[6] Y. M. Mustafah, A. W. Azman, A. Bigdeli, and B. C. Lovell, "An automated face recognition system for intelligence surveillance: Smart camera recognizing faces in the crowd," in *First ACM/IEEE International Conference on Distributed Smart Cameras*, 2007, pp. 147–152.

[7] M. Xu, L. Lowey, and J. Orwell, "Architecture and algorithms for tracking football players with multiple cameras," *IEE Proceedings - Intelligent Distributed Surveillance Systems*, pp. 51–55, 2004.

[8] M. Xu, J. Orwell, L. Lowey, and D. Thirde, "Architecture and algorithms for tracking football players with multiple cameras," *IEE Proceedings - Vision, Image and Signal Processing*, vol. 152, no. 2, pp. 232–241, 2005.

[9] C. Stauffer and W. E. L. Grimson, "Adaptive background mixture models for real-time tracking," in *IEEE Computer Society Conference on Computer Vision and Pattern Recognition*, vol. 2, 1999, pp. 246–252.

[10] J. Krumm, S. Harris, B. Meyers, B. Brumitt, M. Hale, and S. Shafer, "Multi-camera multi-person tracking for easyliving," in *Third IEEE International Workshop on Visual Surveillance*, 2000, pp. 3–10.

[11] M. Fischer and D. Henrich, "Surveillance of robots using multiple colour or depth cameras with distributed processing," in *Third ACM/IEEE International Conference on Distributed Smart Cameras*, 2009, pp. 1–8.

[12] G. Halevi and D. Weinshall, "Motion of disturbances: Detection and tracking of multi-body non-rigid motion," in *IEEE Computer Society Conference on Computer Vision and Pattern Recognition*, 1997, pp. 879–902.

[13] M. J. Swain and D. H. Ballard, "Color indexing," *International Journal of Computer Vision*, vol. 7, no. 1, pp. 11–32, 1991.

[14] R. Campbell and J. Krumm, "Object recognition for an intelligent room," in *IEEE Conference on Computer Vision and Pattern Recognition*, vol. 1, 2000, pp. 691–697.

[15] P. Viola and M. Jones, "Rapid object detection using a boosted cascade of simple features," in *IEEE Computer Society Conference on Computer Vision and Pattern Recognition*, vol. 1, 2001, pp. I–511 – I–518.

[16] H. Detmold, A. van den Hengel, A. Dick, A. Cichowski, R. Hill, E. Kocadag, K. Falkner, and D. S. Munro, "Topology estimation for thousand-camera surveillance networks," in *First ACM/IEEE International Conference on Distributed Smart Cameras*, pp. 195–202.

[17] D. Makris, T. Ellis, and J. Black, "Bridging the gaps between cameras," in *IEEE Computer Society Conference on Computer Vision and Pattern Recognition*, vol. 2, 2004, pp. II–205 – II–210.

[18] N. T. Nguyen, S. Venkatesh, G. West, and H. H. Bui, "Multiple camera coordination in a surveillance system," *Acta Automatica Sinica*, vol. 29, no. 3, pp. 408–421, 2003.

[19] B. Atwood, B. Warneke, and K. S. J. Pister, "Preliminary circuits for smart dust," in *Southwest Symposium on Mixed-Signal Design*, February 2000, pp. 87–92.

[20] B. Warneke, B. Atwood, and K. S. J. Pister, "Smart dust mote forerunners," in *14th IEEE International Conference on Micro Electro Mechanical Systems*, 2001, pp. 357–360.

[21] B. A. Warneke, M. D. Scott, B. S. Leibowitz, L. Zhou, C. L. Bellew, J. A. Chediak, J. M. Kahn, B. E. Boser, and K. S. J. Pister, "An autonomous 16 mm^3 solar-powered node for distributed wireless sensor networks," in *First IEEE International Conference on Sensors*, vol. 2, 2002, pp. 1510–1515 vol 2.

[22] S. E.-A. Hollar, *COTS Dust*. PhD thesis, University of California at Berkeley, 2000.

[23] A. S. Adonin, K. O. Petrosjanc, and I. V. Poljakov, "Monolith optoelectronic integrated circuit with built-in photo-voltaic supply for control and monitoring," in *IEEE International Conference on Electronics, Circuits, and Systems*, vol. 2, 1998, pp. 529–531 vol 2.

[24] W. J. Butera, *Programming a Paintable Computer*. PhD thesis, Massachusetts Institute of Technology, 2002.

[25] I. Chatzigiannakis and S. Nikoletseas, "A sleep-awake protocol for information propagation in smart dust networks," in *International Parallel and Distributed Processing Symposium*, 2003.

[26] S. Nikoletseas, I. Chatzigiannakis, H. Euthimiou, A. Kinalis, A. Antoniou, and G. Mylonas, "Energy efficient protocols for sensing multiple events in smart dust networks," in *37th Annual Simulation Symposium*, 2004, pp. 15–24.

[27] S.-G. Wuu, D.-N. Yaung, C.-H. Tseng, H.-C. Chien, C. S. Wang, Y.-K. Hsiao, C.-K. Chang, and B. J. Chang, "High performance 0.25-um cmos color imager technology with non-silicide source/drain pixel," in *IEEE Electron Devices Meeting Technical Digest, International*, December 2000, pp. 705–708.

[28] G. Agranov, V. Berezin, and R. H. Tsai, "Crosstalk and microlens study in a color cmos image sensor," *IEEE Transactions on Electron Devices*, vol. 50, no. 1, pp. 4–11, 2003.

[29] M. Furumiya, K. Hatano, I. Murakami, T. Kawasaki, C. Ogawa, and Y. Nakashiba, "A 1/3-in 1.3 m-pixel single-layer electrode ccd with a high-frame-rate skip mode," *IEEE Transactions on Electron Devices*, vol. 48, pp. 1915–1921, September 2001.

[30] T.-K. Shin, J.-R. Ho, and J.-W. Cheng, "A new approach to polymeric microlens array fabrication using soft replica molding," *IEEE Photonics Technology Letters*, vol. 16, pp. 2078–2080, September 2004.

[31] S.-K. Lee, K.-C. Lee, and S. Lee, "Microlens fabrication by the modified liga process," in *15th IEEE International Conference on Micro Electro Mechanical Systems*, January 2002, pp. 520–523.

[32] M. Karlsson and F. Nikolajeff, "Diamond micro-optics," in *IEEE/LEOS International Conference on Optical MEMs*, 2002, pp. 141–142.

[33] J. Tanida and K. Yamada, "Tombo: Thin observation module by bound optics," in *IEEE Lasers and Electro-Optics Society*, November 2002, pp. 233–234.

[34] K. Yamada, J. Tanida, Y. Kitamura, and Y. Ichioka, "An opto-electronic image capturing system using multiple-imaging cmos sensor," in *4th Pacific Rim Conference on Lasers and Electro-Optics*, vol. 2, 2001, pp. II–690 – II–691.

[35] T. Nirmaier, C. A. Diez, and J. F. Billie, "High-speed cmos wavefront sensor with resistive-ring networks of winner-take-all circuits," *IEEE Journal of Solid-State Circuits*, vol. 40, pp. 2315–2322, November 2005.

[36] C. W. Jeon, E. Gu, and M. D. Dawson, “Mask-free photolithographic exposure using a matrix-addressable micropixellated alingan ultraviolet light-emitting diode,” *Applied Physics Letters*, vol. 86, pp. 221105 to 221105–3, May 2005.

[37] C.-C. Chen, M.-H. Li, C.-Y. Chang, and G.-C. Chi, “Fabrication of high-na gan diffractive microlenses,” in *IEEE/LEOS International Conference on Optical MEMs*, 2002, pp. 67–68.

[38] C. Hou, M. Li, C. Chen, J. Sheu, J. Chang, G. Chi, C. Wu, W. Cheng, and J. Yeh, “Gan diffractive microlenses for uv micro-optics system,” in *5th Pacific Rim Conference on Lasers and Electro-Optics*, vol. 2, December 2003, p. 715.

[39] P. Herman, J. Li, A. Nejadmalayeri, M. Ng, A. Yick, and J. Ihlemann, “Nano-milling of diffractive optics by f_2-laser ablation,” in *Conference on Lasers and Electro-Optics Europe*, June 2003, p. 557.

[40] S. Enguehard and B. Hatfield, “Continuous beam shaping with optical phased arrays using diffractive optics optimization,” in *IEEE Aerospace Conference*, vol. 3, 2002, pp. 3–1417 – 3–1422.

[41] H. Sagberg, M. Lacolle, I.-R. Johansen, O. Løvhaugen, O. Solgaard, and A. S. Sudbø, “Configurable spectral filter with an array of diffraction gratings,” in *IEEE/LOES International Conference on Optical MEMs*, 2003, pp. 30–31.

[42] H. Sagberg, M. Lacolle, I.-R. Johansen, O. Løvhaugen, R. Belikov, O. Solgaard, and A. S. Sudbø, “Micromechanical gratings for visible and near-infrared spectroscopy,” *IEEE Journal of Selected Topics in Quantum Electronics*, vol. 10, pp. 604–613, May-June 2004.

[43] M. Lacolle, H. Sagberg, I.-R. Johansen, O. Lovhaugen, O. Solgaard, and A. S. Sudbo, “Reconfigurable near-infrared optical filter with a micromechanical diffractive fresnel lens,” *IEEE Photonics Technology Letters*, vol. 17, no. 12, pp. 2622–2624, 2005.

[44] C. Thomas and R. I. Hornsey, “An image sensor with on-die diffractive optics in 0.18 micron bulk cmos,” in *IS&T/SPIE 18th Annual Symposium on Electronic Imaging Science and Technology*, January 2006. Paper no. 6068-06.

[45] C. Thomas and R. I. Hornsey, “A diffractive multispectral image sensor with on- and off-die signal processing and on-die optics in 0.18 micron cmos,” in *IS&T/SPIE 19th Annual Symposium on Electronic Imaging Science and Technology*, January 2007. Paper no. 6501-27.

[46] C. Thomas and R. I. Hornsey, “Mitigating polarization effects in on-die diffractive optics for a cmos image sensor,” in *IS&T/SPIE 20th Annual Symposium on Electronic Imaging Science and Technology*, January 2008. Paper no. 6816-24.

[47] C. Niclass, A. Rochas, P. A. Besse, R. S. Popovic, and E. Charbon, “Cmos imager based on single photon avalanche diodes,” in *13th International Conference on Solid-State Sensors, Actuators, and Microsystems*, vol. 1, 2005, pp. 1030–1034.

[48] B. R. Rae, C. Griffin, J. McKendry, J. M. Girkin, H. X. Zhang, E. Gu, D. Renshaw, E. Charbon, M. D. Dawson, and R. K. Henderson, “Cmos driven micro-pixel leds integrated with single photon avalanche diodes for time resolved fluorescence measurements,” *Journal of Physics D: Applied Physics*, vol. 41, no. 9, p. 094011, 2008.

[49] G. Langfelder, A. Longoni, and F. Zaraga, “The transverse field detector: a cmos active pixel sensor capable of on-line tuning of the spectral response,” in *IEEE Conference on Sensors*, 2009, pp. 1652–1657.

[50] M. Jutzi, M. Grozing, E. Gaugler, W. Mazioschek, and M. Berroth, “2-gb/s cmos optical integrated receiver with a spatially modulated photodetector,” *IEEE Photonics Technology Letters*, vol. 17, no. 6, pp. 1268–1270, 2005.

[51] M. Boulemnakher, E. Andre, J. Roux, and F. Paillardet, “A 1.2v 4.5mw 10b 100ms/s pipeline adc in a 65nm cmos,” in *IEEE International Solid-State Circuits Conference*, 2008.

[52] M. D. Scott, B. E. Boser, and K. S. J. Pister, “An ultralow-energy adc for smart dust,” *IEEE Journal of Solid State Circuits*, vol. 38, no. 7, pp. 1123–1129, 2003.

[53] M. van Elzakker, E. van Tuijl, P. Geraedts, D. Schinkel, E. Klumperink, and B. Nauta, “A 10-bit charge-redistribution adc consuming 1.9 uw at 1 ms/s,” *IEEE Journal of Solid-State Circuits*, vol. 45, pp. 1007–1015, May 2010.

[54] I. Ahmed, J. Mulder, and D. A. Johns, "A low-power capacitive charge pump based pipelined adc," *IEEE Journal of Solid-State Circuits*, vol. 45, pp. 1016–1027, May 2010.

[55] B. Murmann, "Adc performance survey 1997-2010." Available at http://www.stanford.edu/ murmann/adcsurvey.html.

[56] J. K. Her, K. Y. Wang, and Y. H. Chiou, "Tsmc 0.18um logic 1p6m salicide 1.8v/3.3v spice models," tech. rep., Taiwan Semiconductor Manufacturing Co. LTD, 1999.

[57] Y. M. Lin, C. H. Huang, C. P. Hung, and C. C. Ko, "Tsmc 0.18um mixed signal 1p6m salicide 1.8v/3.3v spice models," tech. rep., Taiwan Semiconductor Manufacturing Co. LTD, 2002.

[58] R. Genov and G. Cauwenberghs, "Kerneltron: Support vector machine in silicon," *IEEE Transactions on Neural Networks*, vol. 14, no. 5, pp. 1426–1434, 2003.

[59] R. Karakiewicz, R. Genov, A. Abbas, and G. Cauwenberghs, "175 gmacs/mw charge-mode adiabatic mixed-signal array processor," in *2006 Symposium on VLSI Circuits*, 2006.

[60] R. Karakiewicz, R. Genov, and G. Cauwenberghs, "480-gmacs/mw resonant adiabatic mixed-signal processor array for charge-based pattern recognition," *IEEE Journal of Solid-State Circuits*, vol. 42, no. 11, pp. 2573–2584, 2007.

[61] H. Shin and M. F. Chang, "1.1 gbit/s rf-interconnect based on 10 ghz rf-modulation in 0.18 μm cmos," *IEE Electronics Letters*, vol. 38, no. 2, pp. 71–72, 2002.

[62] H. Shin, Z. Xu, and M. F. Chang, "Rf-interconnect for multi-gb/s digital interface based on 10 ghz rf-modulation in 0.18 μm cmos," in *IEEE MTT-S International Microwave Symposium Digest*, vol. 1, 2002, pp. 477–480.

[63] J. Kim, I. Verbauwhede, and M.-C. F. Chang, "A 5.6-mw 1-gb/s/pair pulsed signaling transceiver for a fully ac coupled bus," *IEEE Journal of Solid-State Circuits*, vol. 40, no. 6, pp. 1331–1340, 2005.

[64] M. F. Chang, V. Roychowdhury, L. Y. Zhang, S. N. Zhou, Z. Y. Wang, Y. C. Wu, P. X. Ma, C. S. Lin, and Z. J. Kang, "Multi-i/o and reconfigurable rf/wireless interconnect based on

near field capacitive coupling and multiple access techniques," in *IEEE 2000 International Interconnect Technology Conference*, 2000, pp. 21–22.

[65] M.-C. F. Chang, V. P. Roychowdhury, L. Zhang, H. Shin, and Y. Qian, "Rf/wireless interconnect for inter- and intra-chip communications," *Proceedings of the IEEE*, vol. 89, no. 4, pp. 456–466, 2001.

[66] D. Salzman, T. Knight, and P. Franzon, "Application of capacitive coupling to switch fabrics," in *IEEE Multi-Chip Module Conference*, 1995, pp. 195–199.

[67] T. F. Knight and D. B. Salzman, "Manufacturability of capacitively coupled multichip modules," in *Proceedings of the 44th Electronic Components and Technology Conference*, 1994, pp. 605–608.

[68] L. A. Hayden and V. K. Tripathi, "Pulse signaling using capacitively-coupled cmos," in *IEEE 3rd Topical Meeting on Electrical Performance of Electronic Packaging*, 1994, pp. 7–9.

[69] T. J. Gabara and W. C. Fischer, "Capacitive coupling and quantized feedback applied to conventional cmos technology," *IEEE Journal of Solid-State Circuits*, vol. 32, no. 3, pp. 419–427, 1997.

[70] J. Xu, J. Wilson, S. Mick, L. Luo, and P. Franzon, "2.8 gb/s inductively coupled interconnect for 3-d ics," in *2005 Symposium on VLSI Circuits*, 2005, pp. 352–355.

[71] N. Miura, D. Mizoguchi, M. Inoue, K. Niitsu, Y. Nakagawa, M. Tago, M. Fukaishi, T. Sakurai, and T. Kuroda, "A 1 tb/s 3 w inductive-coupling tansceiver for 3d-stacked inter-chip clock and data link," *IEEE Journal of Solid-State Circuits*, vol. 42, no. 1, pp. 111–122, 2007.

[72] N. Miura, T. Sakurai, and T. Kuroda, "Crosstalk countermeasures for high-density inductive-coupling channel array," *IEEE Journal of Solid-State Circuits*, vol. 42, no. 2, pp. 410–421, 2007.

[73] K. Misiakos, E. Tsoi, E. Halmagean, and S. Kakabakos, "Monolithing integration of light emitting diodes, detectors, and optical fibers on a silicon wafer: A cmos compatible optical sensor," in *IEEE International Electron Devices Meeting*, 1998, pp. 25–28.

[74] C. Debaes, M. Vervaeke, V. Baukens, H. Ottevaere, P. Vynck, P. Tuteleers, B. Volckaerts, W. Meeus, M. Brunfaut, J. V. Campenhout, A. Hermanne, and H. Thienpont, "Low-cost microoptical modules for mcm level optical interconnectons," *IEEE Journal of Selected Topics in Quantum Electronics*, vol. 9, pp. 518–530, March/April 2003.

[75] L. J. Irakliotis, S. A. Feld, F. R. Beyette, P. A. Mitkas, and C. W. Wilmsen, "Optoelectronic parallel processing with surface-emitting lasers and free-space interconnects," *Journal of Lightwave Technology*, vol. 13, no. 6, pp. 1074–1084, 1995.

[76] W.-Z. Chen, Y.-L. Cheng, and D.-S. Lin, "A 1.8-v 10-gb/s fully integrated cmos optical receiver analog front-end," *IEEE Journal of Solid-State Circuits*, vol. 40, no. 6, pp. 1388–1396, 2005.

[77] J. F. Dickson, "On-chip high-voltage generation in mnos integrated circuits using an improved voltage multiplier technique," *IEEE Journal of Solid-State Circuits*, vol. 11, no. 3, pp. 374–378, 1976.

[78] J.-T. Wu and K.-L. Chang, "Mos charge pumps for low-voltage operation," *IEEE Journal of Solid-State Circuits*, vol. 33, no. 4, pp. 592–597, 1998.

[79] K. Cho, D. Lee, J. Lee, and G. Han, "Sub-1-v cmos image sensor using time-based readout circuit," *IEEE Transactions on Electron Devices*, vol. 57, no. 1, pp. 222–227, 2010.

[80] K. Cho, D. Lee, and G. Han, "Low voltage time based cmos active pixel sensor," in *International SoC Design Conference*, vol. 1, 2008, pp. I–97 – I–100.

[81] S. Lee and K. Yang, "Sub-1-v supply self-adaptive cmos image sensor cell with 86-db dynamic range," *IEEE Electron Device Letters*, vol. 28, no. 6, pp. 492–494, 2007.

[82] C. W. Jeon, H. W. Choi, E. Gu, and M. D. Dawson, "High-density matrix-addressable alingan-based 368-nm microarray light-emitting diodes," *IEEE Photonics Technlogy Letters*, vol. 16, no. 11, pp. 2421–2423, 2004.

[83] H. W. Choi, C. W. Jeon, and M. D. Dawson, "High-resolution 128x96 nitride microdisplay," *IEEE Electron Device Letters*, vol. 25, pp. 277–279, May 2004.

[84] S. J. Chang, C. S. Chang, Y. K. Su, P. T. Chang, Y. R. Wu, K. H. Huang, and T. P. Chen, "Algainp yellow-green light-emitting diodes with a tensile strain barrier cladding layer," *IEEE Photonics Technology Letters*, vol. 9, no. 9, pp. 1199–1201, 1997.

[85] S.-J. Kim, "Improvement of gan-based light-emitting diode by indium-tin-oxide transparent electrode and vertical electrode," *IEEE Photonics Technology Letters*, vol. 17, no. 8, pp. 1617–1619, 2005.

[86] H. Sugawara, K. Itaya, and G. Hatakoshi, "Characteristics of a distributed bragg reflector for the visible-light spectral region using ingaalp and gaas: Comparison of transparent- and loss-type structures," *Journal of Applied Physics*, vol. 74, no. 5, pp. 3189–3193, 1993.

[87] H. Sugawara, K. Itaya, H. Nozaki, and G. Hatakoshi, "High-brightness ingaalp green light-emitting diodes," *Applied Physics Letters*, vol. 61, no. 15, pp. 1775–1777, 1992.

[88] M. Jalonen, J. Kongas, M. Toivonen, P. Savolainen, A. Salokatve, and M. Pessa, "Monolithic super-bright red resonant cavity light-emitting diode grown by solid source molecular beam epitaxy," *IEEE Photonics Technology Letters*, vol. 10, no. 7, pp. 923–925, 1998.

[89] K. H. Kim, J. H. Shin, N. M. Park, T. Y. Kim, C. Hur, K. S. Cho, and G. Y. Sung, "High-extraction-efficiency si-qd led using rugged surface pattern," in *IEEE International Conference on Group IV Photonics*, 2005, pp. 90–92.

[90] H. W. Choi, C. W. Jeon, and M. D. Dawson, "Ingan microring light-emitting diodes," *IEEE Photonics Technology Letters*, vol. 16, no. 1, pp. 1041–1135, 2004.

[91] R.-T. Huang, P. Holm, and P. D. Wright, "Design and fabrication of algainp led array with integrated gaas decode circuits," *IEEE Transactions on Electron Devices*, vol. 45, no. 11, pp. 2283–2290, 1998.

[92] D.-H. Kim and J. A. del Alamo, "Scalability of sub-100 nm inas hemts on inp substrate for future logic applications," *IEEE Transactions on Electron Devices*, vol. 57, no. 7, pp. 1504–1511, 2010.

[93] T. Egawa, B. Zhang, and H. Ishikawa, "High performance of ingan leds on (111) silicon substrates grown by mocvd," *IEEE Electron Deviec Letters*, vol. 26, no. 3, pp. 169–171, 2005.

[94] M. Wakui, R. Ito, H. Sameshima, F.-R. Hu, and K. Hane, "Gan-led grown on si substrate by mbe/mocvd and monolithic fabrication of a light distribution variable device," in *International Solid-State Sensors, Actuators, and Microsystems Conference*, 2009, pp. 1349–1352.

[95] J. C. Gerbedoen, A. Soltani, S. Joblot, J. C. D. Jaeger, C. Gaquiere, Y. Cordier, and F. Semond, "Algan/gan hemts on (001) silicon substrate with power density performance of 2.9 w/mm at 10 ghz," *IEEE Transactions on Electron Devices*, vol. 57, no. 7, pp. 1497–1503, 2010.

[96] R. H. Horng, S. H. Huang, D. S. Wuu, and C. Y. Chiu, "Algainp/mirror/si light-emitting diodes with vertical electrodes by wafer bonding," *Applied Physics Letters*, vol. 82, no. 23, pp. 4011–4013, 2003.

[97] S. A. Ringel, O. Kwon, M. Lueck, J. Boeckl, and E. A. Fitzgerald, "Iii-v/si device integration via metamorphic sige substrates," in *Third International SiGe Technology and Device Meeting*, 2006, pp. 1–2.

[98] A. G. Chynoweth and K. G. McKay, "Photon emission from avalanche breakdown in silicon," *Physical Review*, vol. 102, no. 2, pp. 369–376, 1956.

[99] J. P. Proot, C. Delerue, and G. Allan, "Electronic structure and optical properties of silicon crystallites: Application to porous silicon," *Applied Physics Letters*, vol. 61, no. 16, pp. 1948–1950, 1992.

[100] L. Tsybeskov, K. D. Hirschman, S. P. Duttagupta, and P. M. Fauchet, "An led for silicon-based integrated optoelectronics," in *54th Annual Device Research Conference*, 1996, pp. 150–151.

[101] L. Tsybeskov, S. P. Duttagupta, K. D. Hirschman, P. M. Fauchet, K. L. Moore, and D. G. Hall, "Room-temperature photoluminescence and electroluminescence from er-doped silicon-rich silicon oxide," *Applied Physics LEtters*, vol. 70, no. 14, pp. 1790–1792, 1997.

[102] M. V. Wolkin, J. Jorne, P. M. Fauchet, G. Allan, and C. Delerue, "Electronic states and luminescence in porus silicon quantum dots: The role of oxygen," *Physical Review Letters*, vol. 82, no. 1, pp. 197–200, 1999.

[103] G. Y. Sung, N.-M. Park, T.-Y. Kim, K.-H. Kim, K. S. Cho, and J. H. Shin, "High efficiency silicon visible light emitter using silicon nanocrystals in silicon nitride matrix and transparent doping layer," in *IEEE International Conference on Group IV Photonics*, 2005, pp. 51–53.

[104] G. Y. Sung, N.-M. Park, J.-H. Shin, K.-H. Kim, T.-Y. Kim, K. S. Cho, and C. Huh, "Physics and device structures of highly efficient silicon quantum dots based silicon nitride light-emitting diodes," *IEEE Journal of Selected Topics in Quantum Electronics*, vol. 12, no. 6, pp. 1545–1555, 2006.